Wave Energy Research, Development and Demonstration at Oregon State University

Annette von Jouanne, Ph.D. Alan Wallace, Ph.D. Ken Rhinefrank, B.S.E.E.
Emmanuel Agamloh, Ph.D. Dave Eveland, M.S.M.E.

Oregon State University
Corvallis, OR, USA

SYNOPSIS

The solutions to today's energy challenges need to be explored through alternative, renewable and clean energy sources to enable diverse national energy resource plans. An extremely abundant and promising source of energy exists in the world's oceans [1]. Ocean energy exists in many forms including wave, tidal, thermal, and salinity. Among these forms, significant opportunities and benefits have been identified in the area of wave energy extraction. Research conducted by Oregon State University (OSU) using data from National Oceanic and Atmospheric Administration (NOAA) ocean monitoring buoys, as well as studies by the Electric Power Research Institute (EPRI) have shown that the Oregon coastline presents some of the richest ocean wave energy potentials in the USA [2]-[3]. This complements the existing research of an engineering team at OSU investigating novel direct-drive ocean wave energy extraction devices. In this paper, several aspects of OSU's wave energy extraction research, development and demonstration plans will be presented.

INTRODUCTION

Wave Energy has several advantages over other forms of renewable energy such as wind and solar including higher energy densities, enabling devices to extract more power from a smaller volume at consequent lower costs (e.g. the density of water is about 1000 times that of air). In addition, waves are more "available", an indicator of how often the "waves roll" (for wind, how often the "winds blow"). Wave energy availability is in the 80-90% range, whereas wind availability is in the 30-45% range depending on location. Wave energy is also more predictable, with energy forecast times of greater than 10 hours, thus enabling more straightforward and reliable integration into the electric utility grid to provide reliable power.

A strategic, multidisciplinary wave energy team has been formed at Oregon State University (OSU) investigating novel "direct-drive" wave energy buoys designed to be anchored 1-3 miles offshore, in typical water depths of greater than 100 feet, where the buoys will experience gradual, repetitive ocean swells and be invisible to the naked eye from shore. The Oregon State Wave Energy team's research and development goals are driven by the important issues of survivability, reliability and maintainability, in addition to efficient and high quality power take-off systems. OSU's research focuses on a simplification of processes, i.e. replacing systems employing intermediate hydraulics or pneumatics with direct-drive approaches to allow generators to respond directly to the movement of the ocean by employing magnetic fields for contact-less mechanical energy transmission, and power electronics for efficient electrical energy extraction. OSU is a prime location to conduct ocean wave energy research, noting the following strategic facilities:

- OSU is the home of the USA's highest power university-based energy systems laboratory, the Motor Systems Resource Facility (MSRF), with a 750kVA dedicated power supply and full capabilities to regenerate back onto the grid (See Fig. 1).
- OSU is the home of the O. H. Hinsdale Wave Research Lab (WRL) with world-class wave tank facilities including a 342 ft. wave flume (See Fig. 2).
-

The combination of key facilities at Oregon State University, ongoing successful wave energy research, and the tremendous wave potentials and well-suited coastline off the Oregon coast has led the OSU Wave Energy team to pursue the formation of the national U.S. Wave Energy Research, Development and Demonstration Center in Oregon.

Fig. 1 Oregon State University's Motor Systems Resource Facility (MSRF)

Fig. 2 Oregon State University's O. H. Hinsdale Wave Research Lab

DIRECT-DRIVE WAVE ENERGY APPROACHES

Permanent Magnet Linear Generator Buoy

A linear generator simplifies the overall mechanical design of the drive components by eliminating the complex and inefficient process of converting the linear thrust of the waves to rotational torque by hydraulic means. The proposed buoy employs the vertical motion of ocean waves to power a linear generator. The generator consists of a permanent magnet field system (mounted on the central translator shaft) and an armature, in which the power is generated (mounted on the buoy). The translator shaft is anchored to the sea floor, and the buoy/floater moves armature coils relative to the permanent magnet translator to induce

voltages. The translator shaft consists of an assembly of high permeability steel pole tip pieces (needed for the transfer and direction of flux) and high field strength neodymium-iron-boron magnets (the magnet poles are placed in opposition to effectively concentrate the available flux). The concentrated, two-phase armature coils are wrapped with a spiral of thin electrical lamination steel to provide the flux return path through the generator.
In this design the armature was placed on the "floater" component of the buoy and moves relative to the translator, although the opposite design, an external magnet topology, can also be employed. The chosen design was found to simplify the construction of the axially magnetized machine, and also reduced the diameter/size of the magnets and pole pieces. Consequently the overall dimensions of the machine were reduced. For larger machines, as well as radially magnetized machines, the possibility of using an external magnet topology could be investigated.

An overview of the energy conversion and conditioning process is represented in Fig. 3. The design of the power take off (PTO) from the generator to the load allows for future expansion. The preliminary PTO design consists of a full wave bridge rectifier at the output of each phase of the generator. The two rectifiers are then wired in series to provide the total terminal outputs. A capacitor bank is added to provide a consistent smoothed, rectified voltage.

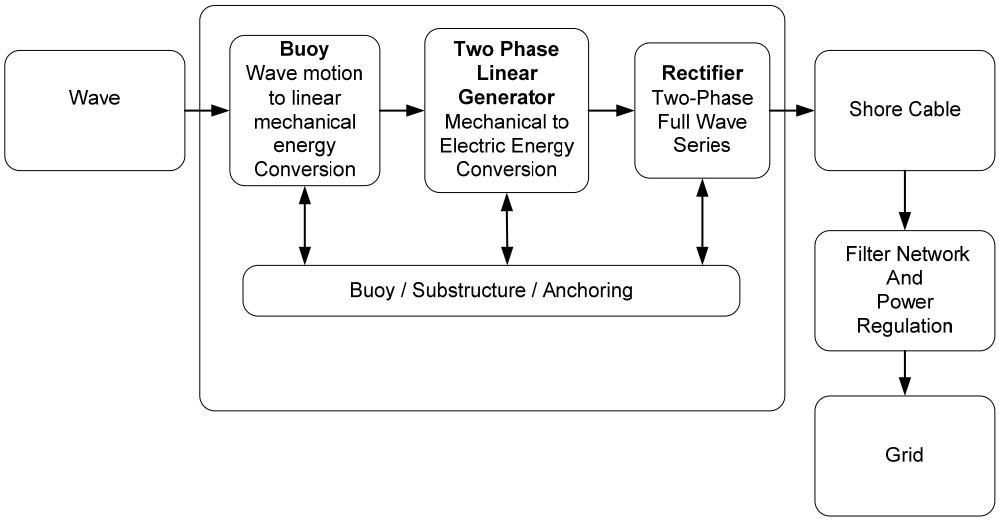

Fig. 3 Permanent Magnet Linear Generator System block diagram

The buoy is a cylindrical spar type, fabricated from a 0.4m diameter, 1.2m long PVC pipe shown in Fig.4. The horizontal cross-like struts that attach the armature to the buoy are made from delrin material and are bolted to the buoy structure, with seals. The buoy is equipped with flange style end caps and a compression spring located at the top of the generator. The spring can be preloaded using a threaded adjustment device placed at the top of the translator shaft and locked with a lock nut; thus enabling the buoy return stroke to be optimized.
Fig. 4 also shows the solid model design of the buoy and internal structural components. The simple buoy design is a deliberate effort aimed at using non-corrosive materials and avoiding too many moving components that would otherwise compromise reliability, and other stringent requirements in an ocean environment.

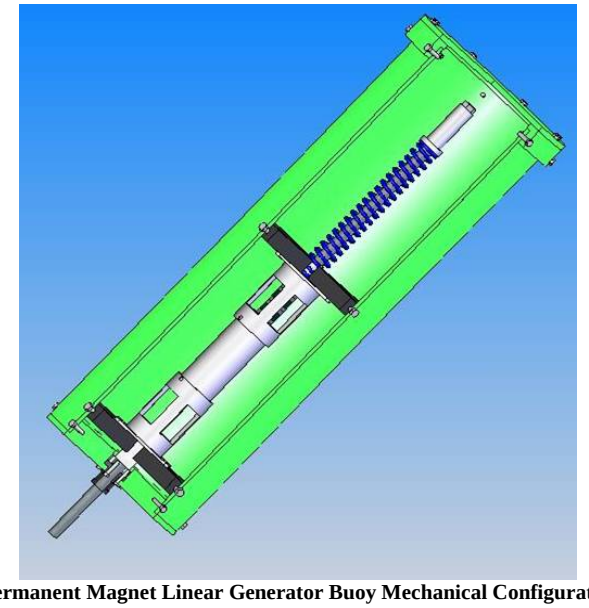

Fig. 4 Permanent Magnet Linear Generator Buoy Mechanical Configuration

The translator is made up of an alternate assembly of 0.010m thick Neodymium-Iron-Boron (Nd-Fe-B) permanent magnets, interspersed with soft iron pole pieces mounted on a threaded aluminium shaft as shown in Fig 5. The magnets are stacked in pairs such that opposing magnetomotive forces (mmfs) drive the flux through the soft iron. Thus, the thickness of each magnet pair and the iron poles are both 0.020m. This results in a pole pitch of 0.040m and the total length of the system is 0.320m. As the armature system moves with respect to the permanent magnet system on the central shaft, its coils experience a change in flux linkage and emf is generated.

The two-phase armature consists of a thin walled tube wrapped with 97 turns of copper magnet wire forming eight individual coil sections. The coil section spacing of 0.020m, combined with a pole spacing of 0.040m results in 90 degrees of phase shift between adjacent coil sections. The coil sections were insulated from each other by means of mica spacers placed between each coil. To provide a return path for the flux, the armature coils are wrapped spirally with thin lamination steel. The steel core is then encased in a cylindrical aluminium shell for mechanical support.

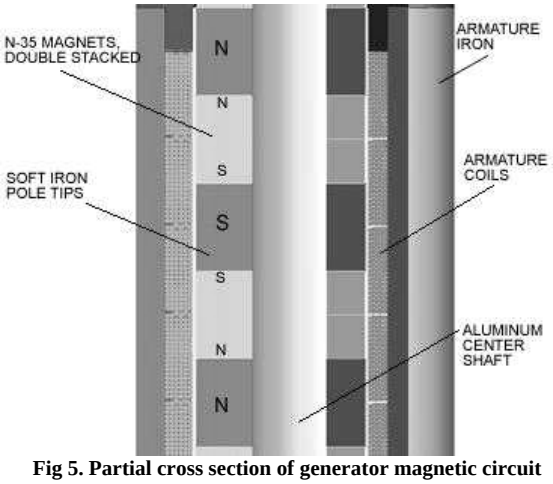

Fig 5. Partial cross section of generator magnetic circuit

This buoy has been demonstrated in both the MSRF and the WRL. To complement these demonstrations, the OSU team is currently designing a linear test bed where controlled reciprocating conditions can be replicated to simulate ocean performance.

Contact-less Force Transmission System

In the severe ocean environment, the power take off (PTO) components must be sealed from exposure and the wave excitation forces, developed by devices such as buoys, have to be transmitted to those sealed components. Here, contactless force transmission system (CFTS) is proposed, which employs magnetic fields for contact-less mechanical thrust transmission. This system has enhanced the design of a new direct drive ocean wave energy converter (OWEC) using ball screw to act as a mechanical gear system for fast speed and torque transmission. The CFTS has been modeled and optimized using Finite Element Analysis (FEA) and the results have been validated with experimental testing in both the MSRF and the WRL. Also, the OWEC has been modeled in Matlab/Simulink using linear wave theory.

The solid model of the overall buoy system is shown in Fig 6 with components such as the CFTS, ball screw and ball nuts displayed in the section view. The system comprises an outer float inside which is a ferromagnetic cylinder which slides against an inner module that contains the PTO components. As the outer float slides, it pulls the piston of the inner module along, with the help of the CFTS. The inner module is completely sealed. The buoyancy force on the outer cylinder is transmitted through the wall of the inner module to the ball nut by the magnetic fields of the CFTS.

Fig 7 shows the actual realization of the overall buoy system displayed in the Motor Systems Resource Facility main testing laboratory. The actual implementation includes an aluminum base plate with three studs on which weights are placed to hold down the buoy during operation. The actual implementation also has the generator located on top of the inner module but it could, in fact, be located at the base of the inner module without any change in performance.

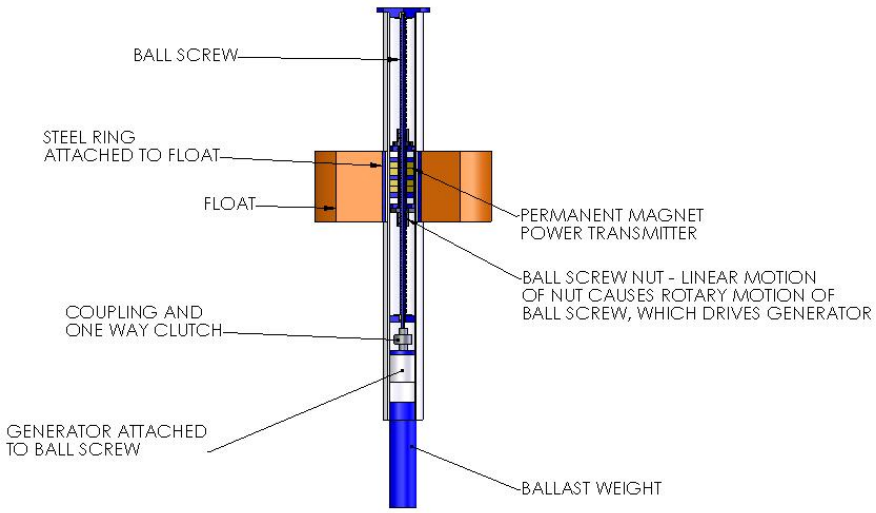

Fig. 6 The Solid Model of the Contactless Force Transmission system Buoy System

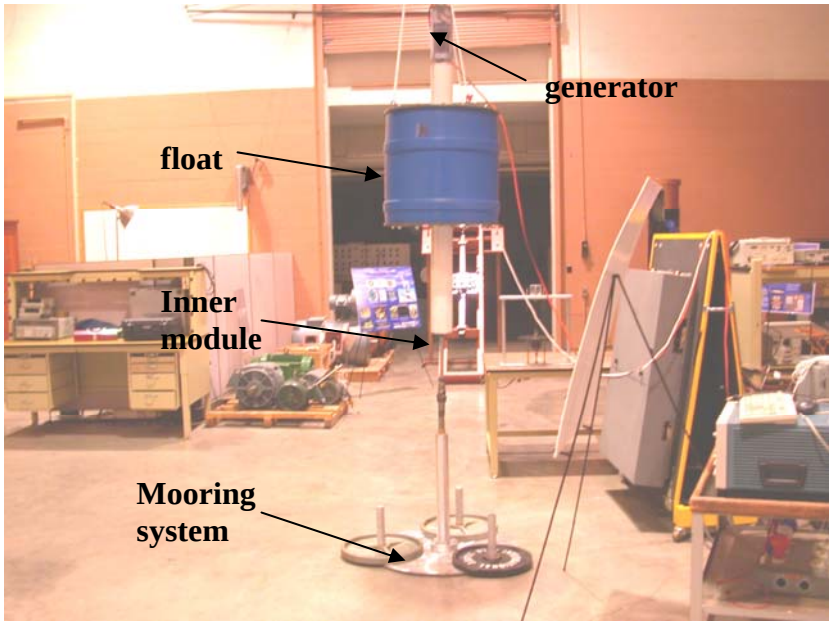

Fig. 7 Prototype of the Contactless Force Transmission system Buoy System

The CFTS is a tubular ferromagnetic reluctance device of two components. The first component consists of neodymium-iron-boron (NdFeB) magnets which are axially magnetized and configured in a "piston" with two opposing poles squeezing magnetic flux radially through a central pole piece into the back-iron "cylinder" (the second component) which is mounted on the buoy. The reluctance force that is developed when the buoy moves up and down is transmitted to the piston through the magnetic field between these two components. The motion of the piston is then transformed to rotation using a roller/ball screw to drive a permanent magnet rotary generator. The entire permanent-magnet piston/ball-screw/generator system is completely sealed and enclosed. As there is no physical contact between the piston and the cylinder, the system will not be damaged if subjected to over loads (such as in storm conditions). It is expected that under such extreme conditions, the system will "slip" and recover when normal sea conditions are restored.

A number of configurations of permanent magnet arrangement and design of the back-iron cylinder were investigated for optimum transmission of thrust as shown in Fig 8. The salient constructions (Designs #2, #3, #4), were better than the non-salient construction (Design #1). Also, the thrust characteristics of Design #2 and Design #3 were not significantly different.

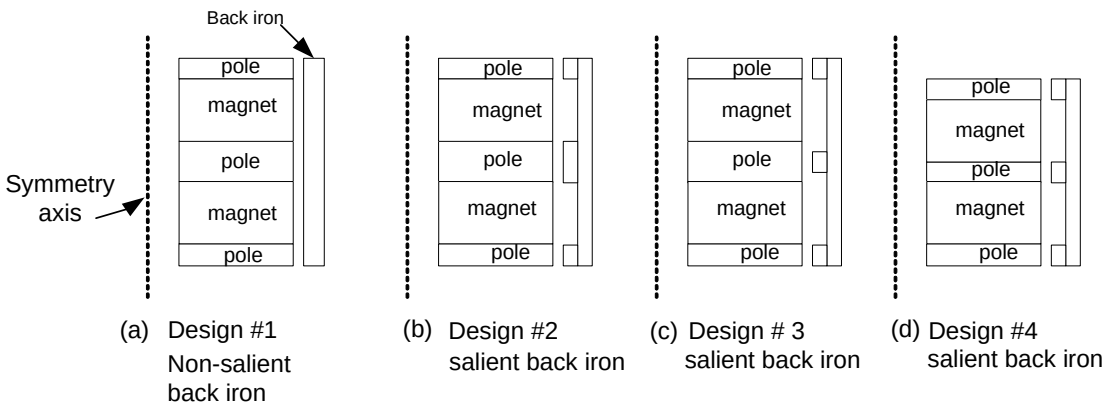

Fig. 8 Design configurations of CFTS

The design of the CFTS progressed through 3 prototype stages. The final design of the piston that was adopted for the OWEC has 4 ring type magnets of following dimensions: external diameter – 100mm, internal diameter – 50mm, axial thickness – 25mm. The magnets were stacked up in pairs per pole piece and interspersed with soft iron ring shaped pole pieces 10mm thick.

Finite element analysis (FEA) has been employed to further investigate alternative Design #2 and #4 as shown in Fig. 9. The main difference between these two configurations is the size of the central pole piece.

In Design #2, the central pole piece is twice the size of the outer pole pieces. In a conventional tubular machine, this would have been the arrangement of pole pieces to create a symmetrical system of equal flux linkage to all phases in order to produce balanced two or three phase voltages. As there are no such requirements in this application, the Design #4, which has all pole pieces of the same size is also possible and has been investigated. It turned out that this design had the highest peak axial thrust as discussed subsequently.

The results of computed force capability as functions of piston-cylinder displacement are given in Fig 10. As shown in the FEA results in Fig 10, the peak thrust of the Design #4 is higher than that of Design #2. The peak thrust is obtained at a displacement approximately equal to one pole dimension. However, the thrust characteristics of Design #2 are wider than that of Design #4, with high thrusts distributed over a wider range of axial displacement.

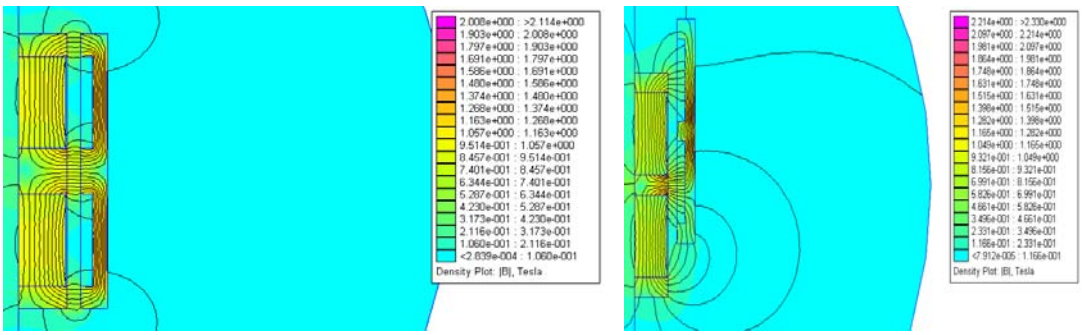

(a) Design #2 **(b) Design #4**

Fig. 9 FEMM 2D Finite Element Modeling

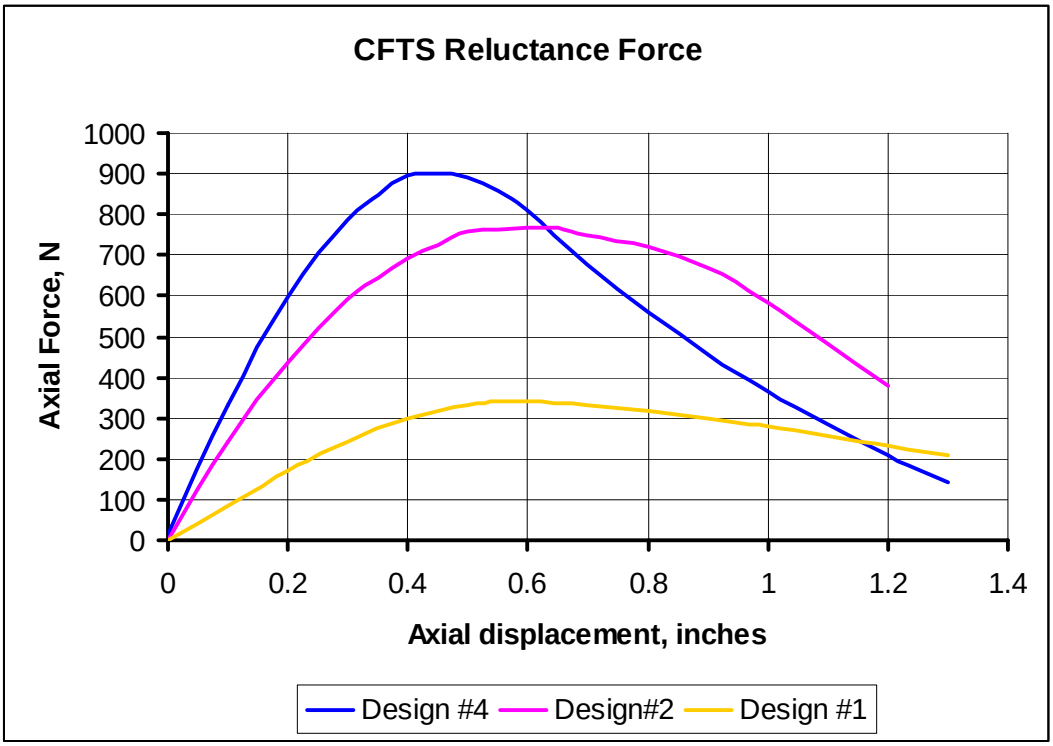

Fig. 10 FEMM 2D axis symmetric computation of Thrust

The difference in the two characteristics is interesting and can be attributed to saturation of the central pole in Design #4 compared to Design #2 and the effects of flux leakage. In Design #4, the effects of saturation of the central pole make the thrust lower compared to Design #2 at higher displacements. On the other hand, the large central pole piece and consequently larger dimensions in Design #2 allow for increased leakage which generally reduces the flux density and thrust. Depending on the required application, either curve can be chosen either to maximize the peak thrust (Design #4) or to allow adequate vertical travel (Design #2).

The laboratory testing of the CFTS was carried out in the MSRF by applying known thrust to the cylinder and measuring the electrical output of the permanent magnet generator. Two permanent magnet generators, shown in Fig. 11, were initially investigated for this project.

(a) Generator #1 **(b) Generator #2**

Fig 11: Permanent Magnet Generators

Generator #1 was the generator intended for use in the buoy. However, in order to increase the travel of the outer float, it was thought that the generator that would be used should fit into the inner module so that the outer float would be able to slide past it. Generator #2 fits well into the inner module and was used for the wave tank testing, though its impedance was very high and there was significant voltage drop across its windings when it is loaded.

The laboratory setup for the testing is shown in the Fig 12. A known thrust is obtained by attaching weights to the outer cylinder and releasing it to accelerate under gravity. The speed measurement was obtained from the oscilloscope capture of the output waveform by measuring its frequency and using equation for the speed of a synchronous generator

$$n_s = \frac{120f}{p}$$

where p is the number of poles and f is the frequency. From the calculated speed, the axial velocity is obtained from the formula $\Omega = \frac{dz}{dt} \cdot \frac{2\pi}{l}$ [rad/s], using the screw lead (l), where Ω is the mechanical speed of rotation of the shaft. The input power to the system is the product of the applied thrust and linear velocity and the output power is measured directly as the electrical power dissipated in the resistances that were connected across the generator.

Fig 12 CFTS, Measurement of conversion efficiency

Figs 13-15 show test result of generator #1 during the laboratory testing to determine the system efficiency. Fig 13 shows the shaft speed of the generator under load and during no load operation. Under no-load, the higher speeds result in higher losses and consequently a non-linear speed-thrust characteristic. Under load, the generator speed is much lower and is more linear with thrust. The current, as expected increases fairly linearly with the applied thrust as shown in Fig 14. The overall system efficiency is greater than 50% for the 10-ohm load but falls as the electrical load is reduced. Similar curves were obtained for generator #2, except that its high impedance resulted in significant voltage drops and lower power output.

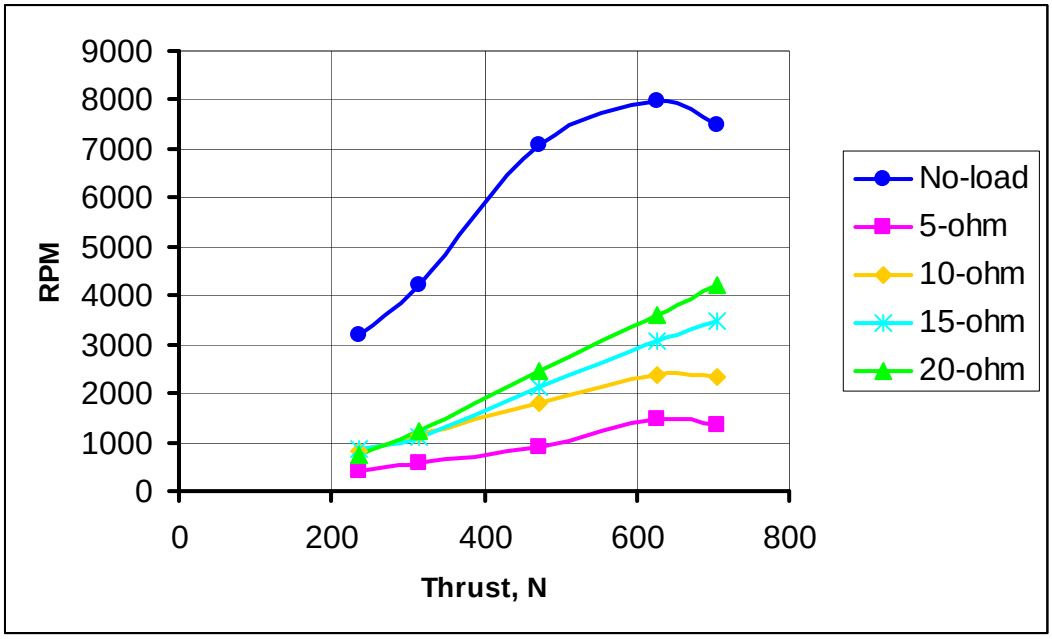

Fig. 13 CFTS System Efficiency

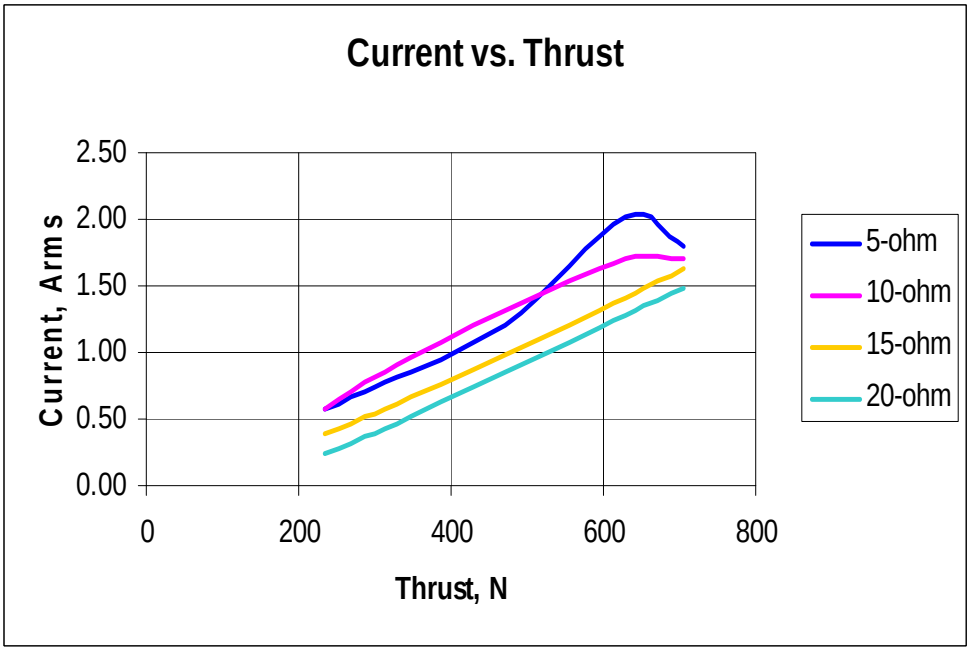

Fig. 14 CFTS Generator Load Current

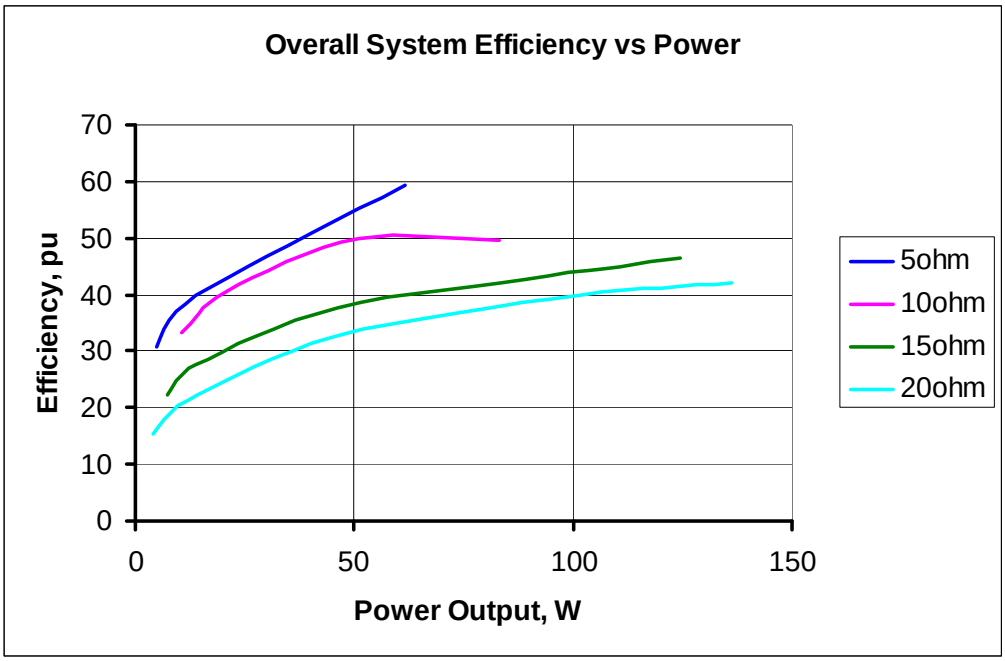

Fig. 15 CFTS System Efficiency

FLUID-STRUCTURE INTERACTION SIMULATIONS

The Analysis of ocean wave energy conversion devices (OWECs) has been largely based on linear potential flow theory in which time domain or frequency domain solutions are obtained usually with assumptions of small amplitude oscillations (linearity). However, practical OWECs require large amplitude oscillations and non-linear effects become an issue. Also, these devices are usually "tuned" to take advantage of resonance. The time domain solutions required have been enhanced with the availability of commercial computational fluid dynamics (CFD) software, to iteratively solve the Navier-Stokes equations. The iterative nature of these fluids solvers also makes it convenient to include the effects of the generators or power take-off mechanisms (PTOs) of the wave energy device, which is generally a non-linear phenomenon.

At OSU, a commercial CFD code has been used to simulate a heaving buoy OWEC, which will be introduced here. The buoy is excited by waves that are generated in a 3D numerical wave tank (NWT) and is free to move in response to the waves. The present work is limited to single degree of freedom heave (SDOF) but can be expanded to include all six degrees of freedom. The fluid-structure interaction (FSI) model also includes modeling the free surface using the volume of fluid (VOF) technique, with the high resolution interface capturing (HRIC) method, which accurately predicts the arbitrary deformation of the air-water interface. The PTO is represented as a damping system across which the energy is captured.

Generally, in a coupled FSI simulation, a fluid dynamics problem is discretized and solved using the fluid flow solver to obtain the forces on the structure. Then the structure motion dynamics is solved using the forces obtained from the fluid solver and other external forces that are pertinent to the problem being solved. The basic mathematical model for the discretization process is the fundamental governing equations of fluid motion, known as the Navier-Stokes (NS) equations. These are a set of equations derived from the conservation laws (mass, energy, momentum, and angular momentum, all of which are conserved in a closed volume). These equations together with the continuity equation constitute the fundamental set of equations that are discretized and solved by the flow solver.

In most engineering problems, there are fluctuations of all the fluid flow quantities in space and time due to turbulence, however, their average values can be considered to be steady. The NS equations that include the effects of turbulence by using the mean fluid flow quantities are known as Reynolds Averaged Navier Stokes Equations (RANSE). In the RANSE the flow quantities are formulated in "Reynold's averaged quantities", by which each dependent variable is expressed as a sum of its time-averaged mean value and a fluctuating component.

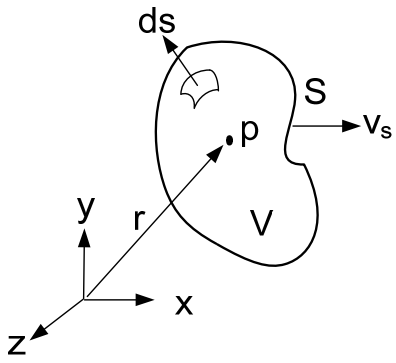

Fig. 16 Control Volume

In integral form the fundamental equations are given by

$$\frac{d}{dt}\int_V \rho u_i dV + \int_S \rho u_i (v - v_s) ds = \int_S (\tau_{ij} - p) ds + \int_V \rho g dV$$

$$\frac{d}{dt}\int_V \rho dV + \int_S \rho (v - v_s) ds = 0$$

where v_s is surface velocity of cell volume, v is continuum velocity, V is a volume bounded by a closed surface S, g is acceleration due to gravity, $\tau_{ij} = \mu_{eff}\left(\frac{\partial u_i}{\partial x_j} + \frac{\partial u_j}{\partial x_i}\right)$ are the effective stresses and μ_{eff} = effective dynamic viscosity of the fluid.

The fluid solver, Comet, is a commercially available unstructured finite volume code. Comet is a general purpose CFD code with efficient set of numerical solution algorithms that can be used to solve both fluid and solid mechanics problems. One feature of the solver that was employed in this work is the ability of the user to generate the grid in blocks with any given blocks not necessarily matching at their interface. Also, there are features that enable two blocks of grid to slide against each other, thus a part of the grid that contains the buoy can be moved or regenerated while the far field grids may remain stationary. The moving of the grid in the fixed global coordinate systems where the RANSE equations are expressed requires the space conservation law, which ensures that the volume of the cells is conserved, even though their shapes change as a result of moving the grid. This law is expressed as

$$\frac{d}{dt}\int_V dV - \int_S v_s ds = 0$$

The numerical 3D solution grid is shown in Fig 17. The overall size of the domain is 12m x 3m x 3m and the cylindrical buoy has a diameter of 0.6m and an equilibrium draft of 0.5m. The mesh is made up of three main blocks; the middle block is a finer mesh that moves with the buoy. This block is regenerated at every time step to maintain its structural integrity as the buoy moves up and down. This buoy-fitted block is flanked on each side by relatively coarse “stationary” meshes that form part of the solution domain but do not form part of the mesh regeneration procedure at each time step. Furthermore, the "stationary” mesh has variable size with larger sizes towards the wall boundaries to provide damping effect of the waves. The numerical grid is generated using the command language of Comet.

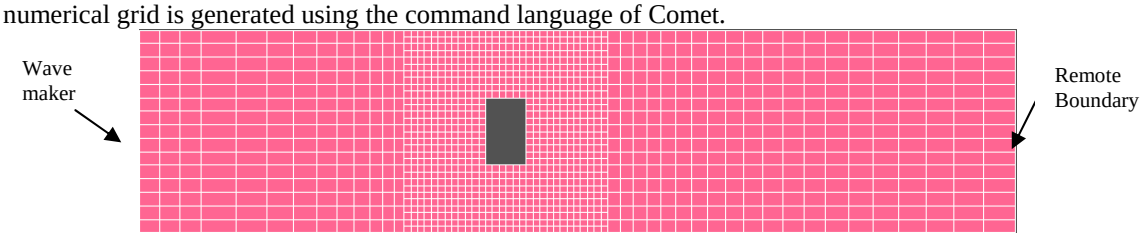

Fig. 17 Numerical Grid

The solution domain is bounded by a wave maker on the left wall boundary. At the wave maker boundary, the horizontal velocity of motion of the boundary is imposed on the water particle velocities at the boundary.

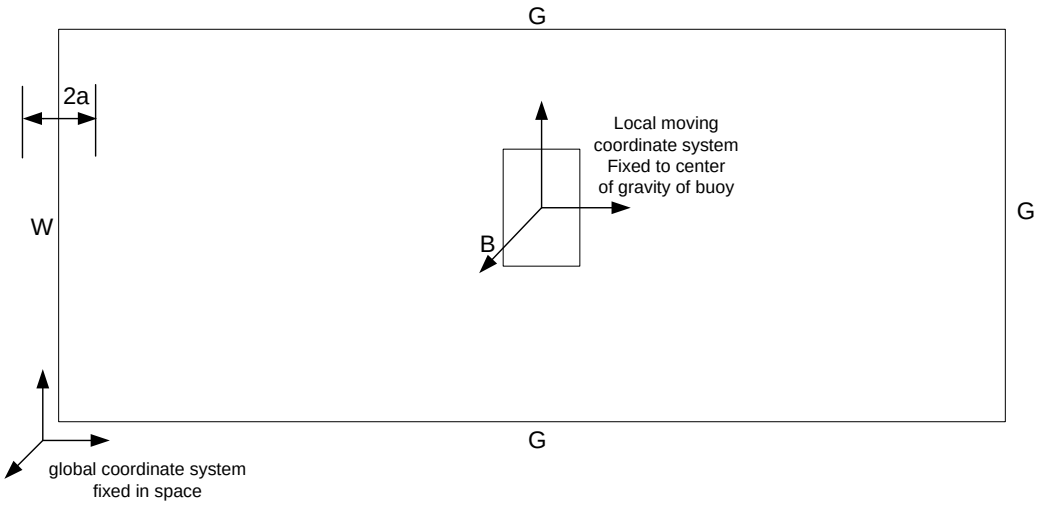

Fig. 18 2D representation of boundaries of solution domain

The other boundaries of the solution domain are solid walls where no-slip boundary conditions are applied. The no-slip condition ensures that the fluid moving over a solid surface does not have velocity relative to the surface at the point of contact. For the floating buoy, the no slip condition also means that the vertical heave velocity is imposed on the water particles at the boundary of the buoy.

The waves were generated by a piston type wave maker located at the left boundary of the solution domain. The plunger moves sinusoidally with the function $s = a \sin \omega t$. For most wave tanks, the opposite end of the wavemaker is a typical beach which absorbs the waves that are generated, in order to prevent their reflection back into the solution domain. This means either non-reflecting boundaries have to be used or a damping/dissipation zone is added to the solution domain for damping the waves. The non-reflecting boundary option was not feasible in the current work and it was thought that adding a damping zone would increase computational demands. Therefore, in this simulation, the far field boundary is located far enough and simulation time is chosen in such a way to avoid such reflections. Also, the cell volumes located towards the boundaries are made larger and this provided some damping of the waves at the boundaries, adequate enough to avoid wave reflections.

In this work, the motion of the wave energy buoy was obtained from the dynamic system solution of the fluid flow interacting with the buoy structure with due consideration of the damping of the PTO. The model employs a technique in which the mesh moves as the buoy heaves. The instantaneous position of the buoy is determined from the set of add-on codes, implemented in FORTRAN. These additional codes interact with the solver to determine the displacements in order to move the buoy to its new position and also to update the boundary conditions. In order to maintain the structural integrity of the fluid mesh, it is regenerated at every time step. For this reason, the solution domain mesh has been generated in a way to enhance mesh regeneration. The grid consists of a fine mesh fitted to the body (regenerated at every time step) and flanked on each side by a relatively coarse mesh that is not regenerated. These blocks are connected together using the explicit connectivity function of the Comet code.

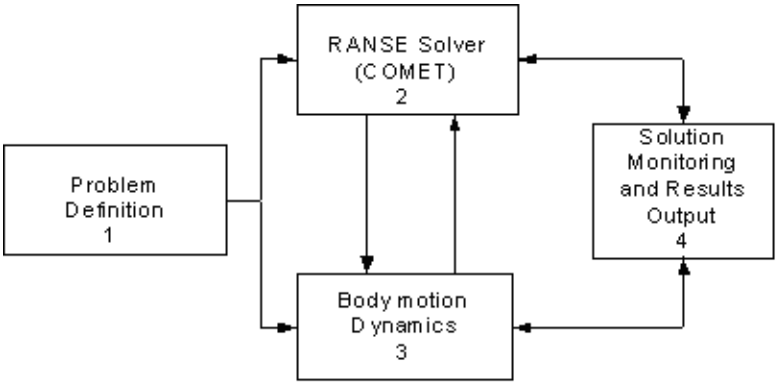

Fig. 19 Block Schematic of Coupling Algorithm

In Fig. 20, the cylindrical buoy is shown in the NWT with a capture of the free water surface at four time instants. The instantaneous power captured by the buoy depends on the PTO damping and the wave conditions. Performance analysis for arrays of multiple buoys is also being conducted.

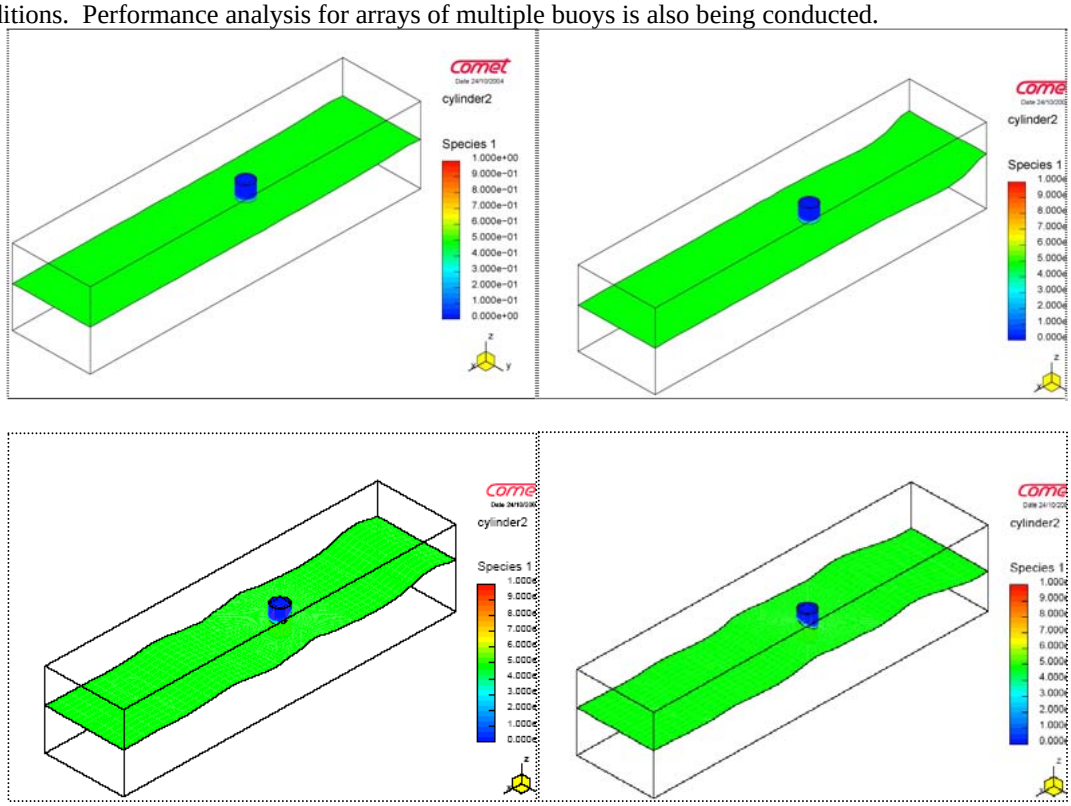

Fig. 20 Free Surface Capturing (single buoy)

CONCLUSION

This paper presented example wave energy work conducted at Oregon State University. Two direct-drive approaches were presented including the permanent magnet linear generator and the contactless force transmission system. Finally, example coupled fluid-structure interaction modeling was presented. There are plans to begin testing of the most promising devices in the ocean in the summer of 2006. Also, the proposed national Wave Energy Research, Development and Demonstration Center is being actively pursued.

REFERENCES

[1] http://www.nrel.gov

[2] A. von Jouanne, A. Wallace, "Conversion of Wave Characteristics to Actual Electric Energy/Power Potentials", Oregon Sea Grant Development Report , submitted January 2004.

[3] G. Hagerman, R. Bedard, M. Previsic "E2I EPRI survey and characterization of potential Offshore Wave Energy sites in Oregon", May 2004.

[4] A. von Jouanne, A. Wallace, H. Zhang, "Preliminary Research on Ocean Energy Extraction Potentials in Oregon", Oregon Sea Grant Development Report, submitted April 25th, 2003

[5] http://www.wavegen.co.uk
[6] http://bigfoot.wes.army.mil/u043.html
[7] http://www.aquaenergygroup.com
[8] http://www.oceanpowertechnologies.com/
[9] http://www.oceanpd.com/
[10] http://www.worldenergy.org/wec-geis
[11] http://acre.murdoch.edu.au/refiles/wave/text.html
[12] http://www.poemsinc.org
[13] http://oregonstate.edu/dept/ncs/newsarch/2002/Dec02/austins.htm
[14] Engineering Committee on Oceanic Resources, Working Group on Wave Energy Conversion. Waves: A Vast Renewable Energy Resource. Publication in preparation.
[15] J. Falnes, "Ocean Waves and Oscillating Systems, Linear Interactions Including Wave-Energy Extraction", Cambridge University Press, 2002.
[16] W. Sweet, E. Bretz, "A National Energy Policy", IEEE Spectrum, July 2001, pp.50-52.
[17] Lethal Loophole, A Comprehensive Report on America's Most Polluting Power Plants and the Loophole that Allows them to Pollute, June 1998.
[18] Buckminster Fuller Institute, http://www.bfi.org/Trimtab/summer01/oceanwave.htm
[19] Australian CRC for Renewable Energy Ltd.
[20] World Energy Council, http://212.125.77.15/wec-geis
[21] Ocean Power Delivery LTD
http://www.oceanpd.com
[22] W.J. Pierson and R.E. Salfi, "The Temporal and Spatial Variability of Power from Ocean Waves Along the West Coast of North America", Wave and Salinity Gradient Energy Conversion Workshop, 1976.
[23] G. McCoy, "Solar Power Plan for the State of Washington – Appendix A", Washington State Energy Office, 1978.
[24] Blue Energy Canada INC, http://www.bluenergy.com
[25] Bigelow Laboratory for Ocean Sciences, http://www.bigelow.org
[26] The Engineering Business Limited, http://www.engb.com
[27] ANSI Standard C84.1–1995, For Electric Power Systems and Equipment – Voltage Ratings (60 Hertz).
[28] IEEE Standard 519-1995, Recommended Practices and Requirements for Harmonic Control in Electrical Power Systems.
[29] Generation Interconnection Development Team, U.S. DOE/BPA Transmission Business Line, "Technical Requirements for the Interconnection of Generation Resources", April 1999.
[30] K. Rhinefrank, E. B. Agamloh, A. von Jouanne, A. K. Wallace, et. al., " A Novel Ocean Energy Permanent Magnet Linear Generator Buoy" 24th ASME Wind Energy Symposium' Reno, Nevada, Jan 10-13, 2005.
[31] M.E. McCormick, Ocean Engineering Wave Mechanics, Wiley, 1973
[32] J. Wang, G.W Jewell, D. Howe, A general framework for the Analysis and Design of Tubular Linear Permanent Magnet machines, IEEE Transactions on Magnetics, Vol.35, No.3, May 1999.
[33] J. Wang, D. Howe, A nalysis of axially magnetized, iron-cored tubular permanent magnet machines, IEE Proceedings of Electric Power Appl, Vol 151, #2, March 2004.
[34] R. W. Yueng and P. Ananthakrishnan, "Oscillation of a floating body in a viscous fluid", J. of Eng. Mathematics, Vol 26., 1992, pp 211-230
[35] T. Sakar, D. Vassalos, " A RANS based technique for simulation of the flow near a rolling cylinder at the free surface" J. of Marine Science and Techn., Vol 5. 2000, pp 66-77.
[36] K. Tanizawa, S. Naito "A study on Parametric Roll Motions by Fully Non-Linear Numerical Wave Tank" Proc 7th ISOPE Conference, May 1997
[37] S. K. Chakrabati, "Hydrodynamics of Offshore Structures" Springer Verlag, 1987
[38] R. G. Dean and R. A. Darymple "Water wave Mechanics for Engineers and Scientists", World Scientific, 1991
[39] G. X. Wu, R. Eatock Taylor, Q. W. Ma, " Numerical Prediction of non-linear loads due to steep waves
[40] A. von Jouanne, A. Wallace, "Investigation of the use of a Novel Roller Screw Concept for Direct Drive Buoys", Oregon Sea Grant Development Report , submitted September 9th , 2004.
[41] A.C. Schacher, "Investigation and Comparison of Generators for Dynamic Operation in Ocean Buoys", M.S. Thesis, Oregon State University, June 2004.
[42] D. Marckx, G. Hjelmeland, A. Wallace, A. von Jouanne "Linear Actuator Using the Switched Reluctance Motor", Final Technical Report – Navy STTR Phase I.